29th EPS Conference on Plasma Phys. and Contr. Fusion Montreux, 17-21 June 2002 ECA Vol. ***26B****, O-2.02 (2002)*

Stability at high performance in the MAST Spherical Tokamak

M. J. Hole, L. C. Appel, R. J. Buttery, M. Grayznevich, K. G. McClements, O. Sauter*, A. Martynov* , A. Thyagaraja and the MAST team.

EURATOM/UKAEA Fusion Association, Culham Science Centre, Abingdon, OX14 3DB, UK.
**CRPP , Association EURATOM-Confédération Suisse, EPFL, 1015 Lausanne, Switzerland.*

1.0 Introduction

The MAST Spherical Tokamak (ST) provides one of the first opportunities to examine the stability properties of the ST in power-plant relevant regimes. This is important in assessing the potential of the ST as a possible route to fusion power. It can also provide crucial tests and data for conventional tokamak physics. High performing regimes are now being routinely accessed on MAST, and their stability properties explored. In this paper, we divide our attention into three stability subjects in MAST: ideal MHD stability limits, Neoclassical Teraing Modes (NTM's), and Alfvenic physics.

2.0 Ideal MHD Stability limits

The ideal n=1 kink instability is likely to set the ultimate performance limit to plasmas in the ST, unless a close fitting conducting wall and active feedback system is introduced into the device. Here, ideal n=1 external kink mode stability limits have been investigated in MAST using the finite element code KINX [1], which computes linear ideal MHD growth rates and eigenvectors of axi-symmetric plasmas surrounded by a vacuum layer and a conducting wall. For the stability calculations, three codes were used to compute the equilibrium: EFIT [2], which computed the experimental equilibrium using magnetic and kinetic constraints; CHEASE [3], which computed a higher resolution equilibrium; and CAXE [4], which was used to remap the equilibrium into a KINX input file. To calculate the stability of an EFIT computed equilibrium, CHEASE took the edge as the flux surface at normalized poloidal flux ψ_n=99.5% of the EFIT last closed flux surface. The radial electron pressure profile was taken from Thomson scattering data. Calculations from LOCUST [5] suggest that in MAST, the fast ion pressure profile comprises no more than ~20% of the total pressure. In this work we have assumed that the ion and electron pressure profiles are the same. To calculate the marginal stability boundaries, the pressure p and flux surface averaged current density I^* profiles were remapped by: $p_1(\psi_n)\rightarrow\gamma p_0(\psi_n)$, $I_1^*(\psi_n)\rightarrow I_0^*(\psi_n^t)$, and the pressure multiplier γ raised until the resultant equilibrium was unstable. For each γ, a shooting method was used to adjust the power index t until the on-axis safety factor, $q(0)$=1.1. Together with the constraint of the total plasma current, this ensured an approximately constant q profile.

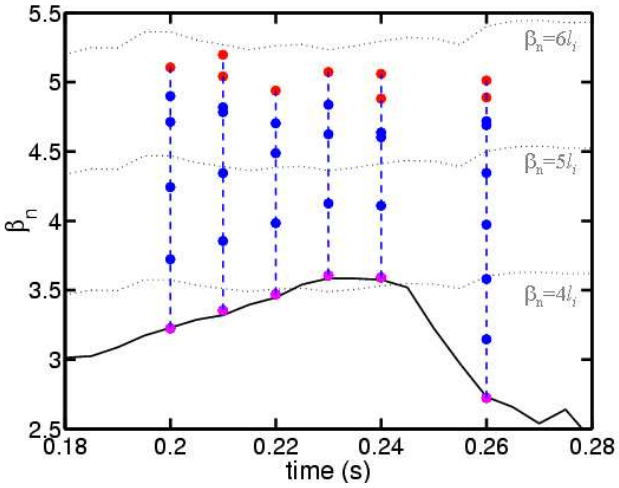

Figure 1: *Time trace of β_n for shot 6271, together with stability trajectory for stable (•,γ=1), (•,γ>1) and unstable (•,γ>1) points.*

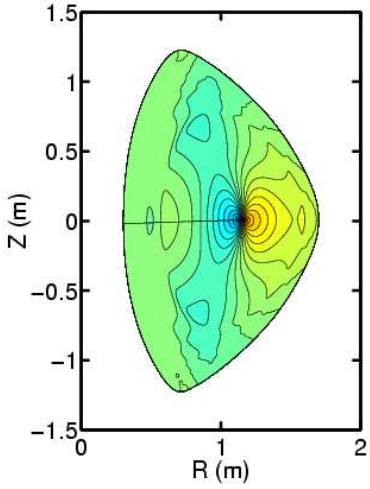

Figure 2: *Normal displacement lines for marginally unstable n=1 external kink mode at 210ms*

Figure 1 is a time trace plotting the normalized beta, β_n for shot 6271. Here, $\beta_n = \beta_t$ (%)/I_n : defined in terms of the toroidal beta, $\beta_t = 2\mu_0 \langle p \rangle / \langle B_0^2 \rangle$, with B_0 the vacuum toroidal magnetic field at the geometric axis and the brackets denoting volume average; and the normalized plasma current $I_n = I_p/(a\ B_0)$, where a is the minor radius. For each point in Fig. 1 the KINX stability computation has been performed, and the point colour coded for stability [γ=1 (magenta), or γ>1 (blue)] or instability (red). The dotted line shows different multiples of the plasma inductance, l_i. By inspection, the stability limit lies around $\beta_n = 5.5 l_i$, approximately 25% above the highest β_n reached in MAST to date. Figure 2 is a plot of the normal mode displacement of the marginally unstable n=1 external kink mode at 210ms. The figure shows that the outboard displacement (yellow) is large with respect to the inboard displacement (blue). Near the geometric centre, the perturbation is predominantly m=1, whilst near the edge the perturbation is predominantly m=2. Numerical convergence tests have been performed, which verify convergence of the eigenvalues to marginal stability and instability at a (r,θ) grid of greater than 150x150 points. Preliminary calculations confirm the mode is stabilized with a conformal wall at ~40% of the minor radius.

Figure 3 is a grey-scaled histogram plot of β_n vs. l_i. of the MAST operating space. Overlaid is the trajectory to instability of the no-wall n=1 external kink mode. The plots show that the present MAST operating space is well below the hard ideal n=1 MHD limit. Finally, Fig. 4 plots the trajectory to instability as a function of pressure peaking factor. The slight decrease in pressure peaking factor ($p(0)/\langle p \rangle$) with increasing β_n is a result of increasing Shafranov shift. Overlaid on Fig. 4 are ideal n=1 external kink mode, no wall stability limit calculations by Menard *et. al.* [6] for aspect ratio A=1.5, q(0), and q*/q(0)=1.5,3.0, where q* is the cylindrical kink safety factor [6]. The calculations are in good agreement with the MAST case studied here, with A=1.42 and q*/q(0)=2.55. Finally, the data points are values of β_n vs. pressure peaking factor, calculated by rerunning EFIT with pressure constrained to the TS data.

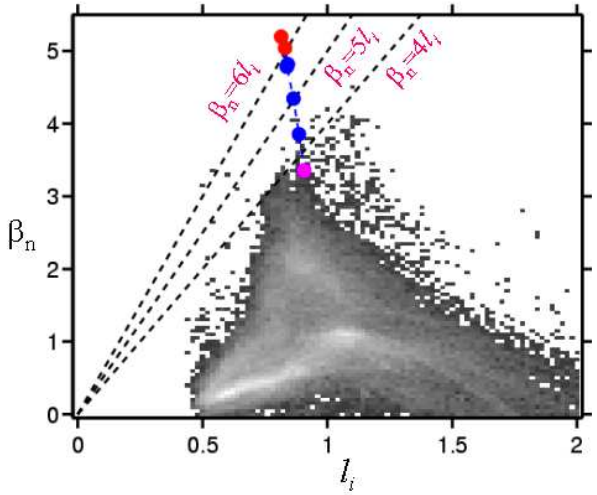

Figure 3. *Histograms of β_n vs. l_i. of the MAST operating space, together with stability trajectory of shot 6271 (see legend of Fig. 1).*

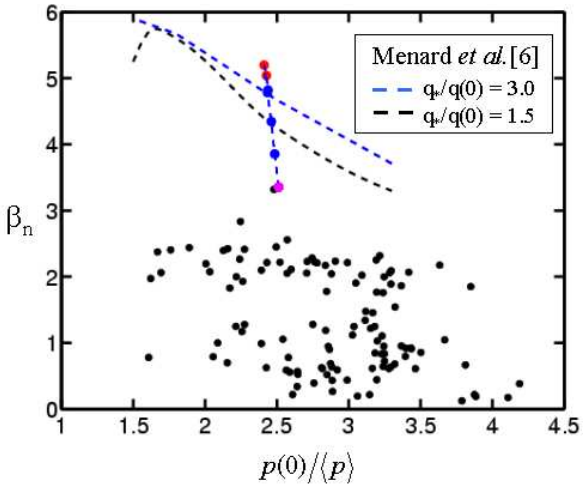

Figure 4: *Stability trajectory of shot 6271 at 210ms (see legend of Fig. 1). Overlaid are no-wall stability limits calculated by Menard et al.* [6]*, and kinetically constrained EFIT MAST data (•).*

3.0 Neoclasssical Tearing Modes

Whilst the ideal n=1 ideal kink instability may set the ultimate performance limit in the ST, the practical limit to performance for many conventional tokamak scenarios is posed by the NTM. Aspect ratio is a key parameter for this mode, entering into the various physics terms governing behaviour in different ways. Thus the ST provides an ideal testing ground for NTM physics models. NTM modes have been identified in the ST on MAST, first reported by Buttery *et al.* [7]. Their behaviour validates the underlying physics models, not only matching the expected trends and effects, but consistent with detailed numerical

predictions for key physics parameters. The modelling also highlights the strong role of field curvature effects for the ST, as predicted by Kruger *et al.* [8], with fits from MAST consistent with a 60% stabilisation of the bootstrap drive [9]. As the ratio of bootstrap drive to field curvature effects scales as $\sqrt{\varepsilon}\,\beta_p\, s\,/\,\beta$, where s is the magnetic shear, this indicates a possible new route for avoidance of these instabilities in the ST, via further optimisation of profiles or variation in q. In addition, the ST's naturally high shaping enables operation with higher q(0), thus removing rational surfaces associated with either the seeding physics or the NTM itself.

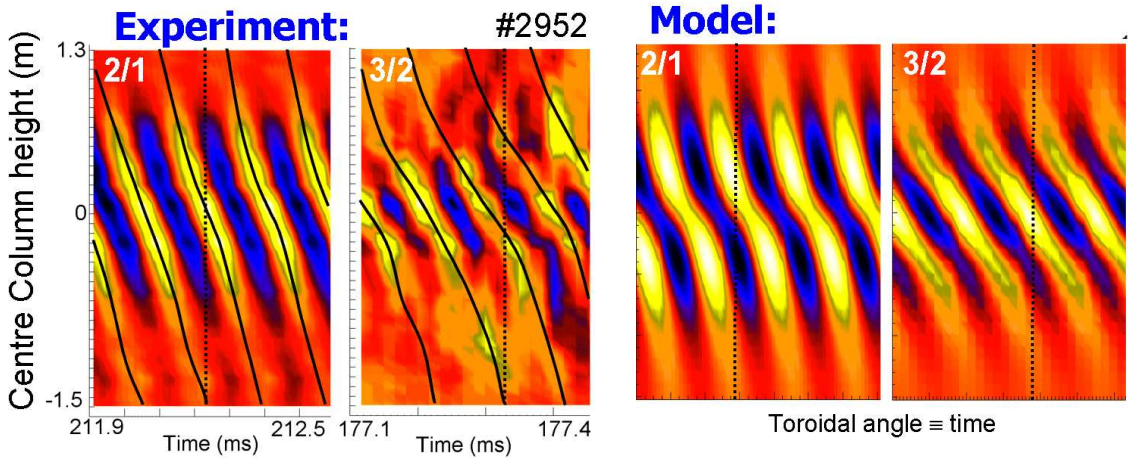

Figure 5: *Observed and predicted mode structure on centre column magnetic array for shot 2952.*

In further work, geometry corrections for the previous cylindrical estimates of island size have been obtained by three-dimensional field modelling. Here, the island is represented as a toroidally-sinusoidal sheet current perturbation, matching the measured magnetic amplitude and consistent with the observation of a single dominant harmonic from magnetics. Field lines were followed in full 3D geometry to measure the vacuum solution island sizes, showing 3/2 island sizes, (typically ~4cm) are very similar to the cylindrical approximation, while 2/1 islands (~8cm) are only ~25% lower than the cylindrical estimates. This modelling has also been used to test measurements of poloidal mode numbers, previously deduced from centre column vertical array. The model confirms that the majority of the modes' structures are observed on the inboard size, and correct identification of the modes as shown in Fig. 5. These estimates are now confirmed by new measurements using the 300 point Thomson scattering diagnostics, which shows structures at q=2 of similar scale to the island sizes predicted by magnetically based estimates for a 2/1 tearing mode in shot 6326 , as shown in Fig. 6.

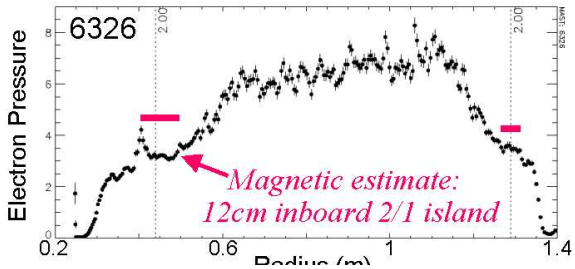

Figure 6: *TS electron pressure for shot 6326.*

4.0 Alfvénic activity

Discrete activity in the range 80kHz to 450kHz has been observed in neutral beam injection (NBI) heated discharges using both H^+ and D^+ co-injection with beam energies exceeding 35keV. A spectrogram of high-frequency activity for shot 4396 is shown in Fig. 7. At the time of the observed activity: I_p=600kA, B_0=0.4T, A=1.9, triangularity δ=1.5 and $v_{\|}/v_A \cong 1.7$ ($v_{\|}$ is the beam velocity and v_A is the Alfvén velocity at the magnetic axis). Discrete activity is observed from around 15ms after the start of the1MW H^+ NBI and continues until just after an internal reconnection occurring at 151ms. The high frequency activity occurs in two frequency ranges consistent with TAE activity $f_{TAE}=v_A/4\pi Rq \cong 175$kHz, and with EAE activity

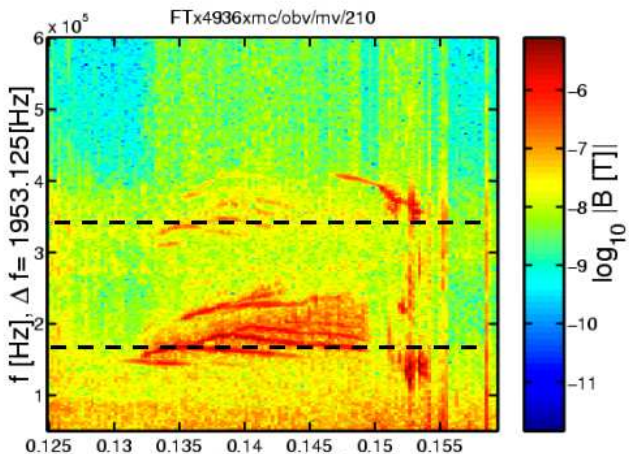

Figure 7: *Spectrogram of an outboard mirnov coil for shot 4936 during NB-heating. Discrete modes occur first in the TAE gap (~170kHz) and from 147ms in the EAE gap (~350kHz).*

$f_{TAE}=v_A/2\pi Rq\cong$350kHz, where R is the radius of the magnetic axis, and q taken to be one. Continuous Alfvén spectra, computed using CSCAS [10], indicate TAE and EAE gaps for low-n modes (n<5). Calculations using the non-linear hybrid MHD guiding centre code HAGIS [11] predict the most unstable toroidal modes are in the range n=4 to n=6. Figure 8 shows an n=3 EAE eigenfunction computed by the ideal MHD code MISHKA-1 [12]. The stronger toroidal coupling in a spherical tokamak results in more than 2 dominant poloidal harmonics.

High frequency Alfvénic activity has also been observed in ohmic plasmas. The activity is generally at a very low ampltiude with mode number n=0, consistent with the excitation of n=0 global Alfvén eigenmodes and low poloidal mode number [13]. Simulations using the 2-fluid turbulence code CUTIE[14] suggest the high frequency is correlated with long-timescale MHD events such as IREs or ELMs. There is no observed effect of these modes on plasma performance but they may be useful as a diagnostic.

5.0 Conclusions

We have investigated three stability subjects in MAST. Ideal MHD calculations have shown that there is scope for at least a rise of 25% in normalized beta, β_n, in MAST before reaching the hard, n=1 external kink mode limit. In future, time resolved TS data and higher NBI beam power will provide scope to further probe beta limits in MAST. Secondly, we have reviewed recent progress in NTM physics, and suggested routes to stabilziation in the ST. In this work, we have modelled the measured magnetic amplitudes with toroidally sinusoidal sheet perturbation, predicting island sizes similar to cylindrical estimates. Similar island sizes have been seen in profiles from 300 point TS scattering diagnostics. Thirdly, we have reported on high frequency Alfvénic activity in Ohmic plasmas, at low amplitude with n=0, consistent with excitation of GAE modes. Finally, we presented evidence of beam-driven EAE activity in MAST. Measured frequencies agree with computed locations of the EAE gap in the Alfven continuum. Drive calculations suggest the most unstable EAE modes are in the range n=4 to n=6. Computations of an n=3 EAE eigenfunction show the presence of more than 2 dominant poloidal harmonics.

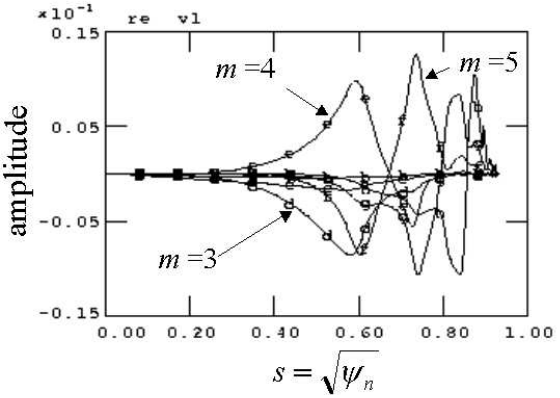

Figure 8: *An EAE eigenfunction with n=3 computed using MISHKA-1[12].*

This work was jointly funded by the U.K. Department of Trade and Industry and EURATOM. O. S. is supported in part by the Swiss National Science Foundation. Special thanks to Dr. S. Medvedev, Keldysh Ins. of Applied Math.for assistance with the stability calculations.

[1] L. Degtyarev *et al.* Comp. Phys. Com.. **103**, (1997).
[2] L. Lao *et al*. Nuc. Fus. **30** pp 1035, (1982).
[3] H. Lutjens *et al.* Comput Phys Commun **97**, 219, (1996).
[4] S. Medvedev *et al.* 20th EPS, (1993).
[5] R. J. Akers *et. al.* Nuc. Fus. **42**, pp122-135, (2002).
[6] J. E. Menard *et al.* Nuclear Fusion, **37**(5), (1997).
[7] R. J. Buttery et al., Contr. Fus. Plas. Phys. **25A** pp. 597, (2001)
[8] S. E. Kruger *et. al.*, Phys. Plas. **5**, 455, (1998).
[9] R. J. Buttery *et al.*, Phys. Rev. Lett. **88,** 125001 (2002).
[10] S. Poedts, E. Schwarz, Journ Comp Phys, 105, 165 (1993).
[11] L. C. Appel *et al,* 7th IAEA, Göteborg (2001).
[12] A. B. Mikhailovskii *et al.*, Plas. Phys. Rep, 23, 844 (1997).
[13] K. G. McClements *et al*., submitted to Nuclear Fusion (2002).
[14] A. Thyagaraja, Plas. Phys. and Cont. Fusion, **42**,B255 (2000).